Antagonistic Coevolution of MER Tyrosine Kinase Expression and Function

Amanda L. Evans, Jack W.D. Blackburn, Kyle Taruc, Angela Kipp, Brennan S. Dirk, Nina R. Hunt, Stephen D. Barr, Jimmy D. Dikeakos, and Bryan Heit*

Department of Microbiology and Immunology and the Centre for Human Immunology, The University of Western Ontario, London, Canada

*Corresponding author: E-mail: bheit@uwo.ca.

Associate editor: Thomas Leitner

Abstract

TYRO3, AXL, and MERTK (TAM) receptors are a family of receptor tyrosine kinases that maintain homeostasis through the clearance of apoptotic cells, and when defective, contribute to chronic inflammatory and autoimmune diseases such as atherosclerosis, multiple sclerosis, systemic lupus erythematosus, rheumatoid arthritis, and Crohn's disease. In addition, certain enveloped viruses utilize TAM receptors for immune evasion and entry into host cells, with several viruses preferentially hijacking MERTK for these purposes. Despite the biological importance of TAM receptors, little is understood of their recent evolution and its impact on their function. Using evolutionary analysis of primate TAM receptor sequences, we identified strong, recent positive selection in *MERTK*'s signal peptide and transmembrane domain that was absent from *TYRO3* and *AXL*. Reconstruction of hominid and primate ancestral *MERTK* sequences revealed three nonsynonymous single nucleotide polymorphisms in the human *MERTK* signal peptide, with a G14C mutation resulting in a predicted non-B DNA cruciform motif, producing a significant decrease in MERTK expression with no significant effect on MERTK trafficking or half-life. Reconstruction of *MERTK*'s transmembrane domain identified three amino acid substitutions and four amino acid insertions in humans, which led to significantly higher levels of self-clustering through the creation of a new interaction motif. This clustering counteracted the effect of the signal peptide mutations through enhancing MERTK avidity, whereas the lower MERTK expression led to reduced binding of Ebola virus-like particles. The decreased MERTK expression counterbalanced by increased avidity is consistent with antagonistic coevolution to evade viral hijacking of MERTK.

Key words: **TAM receptors, MERTK, efferocytosis, antagonistic coevolution, positive selection, viral infection.**

Introduction

The TAM (TYRO3, AXL, and MERTK) receptors are a family of receptor tyrosine kinases that mediate efferocytosis, the phagocytic removal of apoptotic cells (ACs). Although TAM receptors are broadly expressed, the highest expression is observed in the nervous, vascular, reproductive, and immune systems, frequently on resident immune cells and epithelia (Lemke and Rothlin 2008). Like many phagocytic receptors, TAM receptors do not directly bind to their targets and instead are bridged to phosphatidylserine (PtdSer) on the surface of ACs by soluble protein opsonins such as protein S (PROS) and growth arrest-specific 6 (GAS6) (Graham et al. 2014; Tsou et al. 2014). In addition to their role in mediating efferocytosis, TAM receptors can also be hijacked by enveloped viruses such as Ebola and West Nile Virus for cell entry and induction of immunosuppressive signaling, and during cancer can reduce tumor immunogenicity through antiinflammatory signaling and sequestration of tumor antigens (Bhattacharyya et al. 2013; Nguyen et al. 2014; Dahlmann et al. 2015). The three TAM receptors arose early in metazoan evolution through whole genome duplication, emerging from a single ancestral gene found in urochordata, cephalochordate, and hemicordata (Brunet et al. 2016; O'Leary et al. 2016). Despite their distant evolutionary origins, all three TAM receptors retain a high degree of structural and functional similarity, and a modest degree of sequence homology. Although structurally and functionally similar, in mice and humans MERTK is the most critical of the three family members. In humans, mutations resulting in a total loss of *MERTK* cause retinitis pigmentosa, a form of congenital blindness driven by the accumulation of apoptotic outer segments of retinal pigment epithelial cells (Brea-Fernández et al. 2008). Moreover, single nucleotide polymorphisms (SNPs) in *MERTK* contribute to a range of chronic inflammatory and autoimmune diseases, most notably atherosclerosis and multiple sclerosis (Hurtado et al. 2010; Binder et al. 2016; Healy et al. 2016). *MERTK* knockout mice have a severe phenotype, with total deficiency resulting in congenital blindness, susceptibility to atherosclerosis and autoimmunity, and male infertility. In contrast, few SNPs in *AXL* or *TYRO3* are associated with human diseases, and *AXL* and *TYRO3* knockout mice are phenotypically normal (Duncan et al. 2003; Li et al. 2013). Indeed, the triple-TAM knockout mouse has a nearly

Article

identical phenotype to the *MERTK* knockout mouse, albeit with an accelerated development of pathology, consistent with a dominant role for MERTK over the other TAM family members (Chen et al. 2009; Li et al. 2013).

TAM receptors are type I transmembrane glycoproteins, comprised of an extracellular domain containing tandem immunoglobulin-related domains and tandem fibronectin type III repeats, and a protein kinase c-like intracellular kinase domain. TYRO3 and AXL are comparable in size at ~120 kDa (890 and 894 amino acids, respectively), whereas MERTK is significantly larger at ~150–170 kDa (999 amino acids), mainly due to expansion of the ectodomain (Graham et al. 1994; Linger et al. 2008). The kinase domain is highly conserved between TAM family members (>70% identity), and contains a unique KW(I/L)A(I/L)ES active site that differs from other receptor tyrosine kinases (Graham et al. 1994; Lemke and Rothlin 2008; Linger et al. 2008). TAM receptors are activated by homodimerization induced by interactions with the carboxy-terminal domains of ligand-bound opsonins, which stabilize the TAM dimer to initiate signaling (Sasaki et al. 2006). Although TAM signaling remains to be fully elucidated, it is established that TAM dimerization leads to autophosphorylation in the kinase and C-terminal tail domains, resulting in kinase activation and recruitment of SH2-domain bearing proteins which are then phosphorylated by the active kinase domain. SH2 bearing proteins recruited to active TAM receptors include Growth factor receptor-bound protein 2 (GRB2) and the p85α subunit of phosphoinositide-3-kinase (PI3K), activating downstream signaling through PI(3,4,5)P_3, MAPKs, and Rho family GTPases (Tibrewal et al. 2008; Weinger et al. 2008; Shelby et al. 2013). Combined, these signaling pathways enable the large-scale actin and membrane reorganization required to engulf large particles such as ACs. In addition, activation of GRB2 and PI3K also induces expression of Suppressor of Cytokine Signaling 1 and 3 (SOCS1, SOCS3), thus initiating an antiinflammatory program which maintains the tissue in an uninflamed state and prevents initiation of adaptive immune responses (Lee et al. 2012; Zhang et al. 2016). This signaling cascade is critical for maintaining tissue homeostasis, but can be hijacked by some enveloped viruses and cancers to evade the immune system (Morizono et al. 2011; Bhattacharyya et al. 2013; Nguyen et al. 2014; Dahlmann et al. 2015; Kimani et al. 2016).

Despite the strong associations of TAM receptors with a variety of human diseases and the important roles of TAM receptors in immunity, cancer and infectious diseases, the evolutionary history of TAM receptors remains unknown. As such, we performed an evolutionary analysis of the TAM receptors, identifying two regions of intense positive selection in MERTK, but not the other TAM receptors. The pattern of evolution observed in *MERTK* was unusual, as positive selection resided predominantly in the signal peptides and transmembrane domains (TMD); regions which are typically conserved. Functional MERTK assays revealed that the evolution of the signal peptide reduced MERTK expression, whereas the evolution of the TMD acted to maintain MERTK activity through increased avidity while decreasing enveloped virus binding. Combined, these results are consistent with antagonistic coevolution of MERTK but not the other TAM receptors. Antagonistic coevolution is a common form of host-pathogen evolution in which the evolution of a selective advantage in a host species comes at the cost of reduced pathogen fitness. This necessitates a counter-adaptation in the pathogen, thereby restoring pathogenicity and reducing the fitness of the host. This results in an evolutionary arms race, in which the host and pathogen must engage in a continuing cycle of adaptation/counter-adaptation simply to maintain fitness (Paterson et al. 2010; Nordbotten and Stenseth 2016).

Results

Patterns of Recent TAM Receptor Evolution

The three members of the TAM family—TYRO3, AXL, and MERTK—share a common protein structure consisting of an N-terminal signal peptide followed by tandem immunoglobulin-related motifs, tandem fibrinogen type III motifs, a TMD, and an intracellular tyrosine kinase. By analyzing the rates of nonsynonymous (Ka) versus synonymous (Ks) codon replacement, residues under purifying and positive selection can be detected (Doron-Faigenboim et al. 2005). Ka/Ks analysis was performed using evolutionary trees constructed using all available primate sequences for *TYRO3*, *AXL*, and *MERTK*, using stringent Ka/Ks thresholds which only score residues as positively (Ka/Ks > 1.5) or negatively (Ka/Ks < 0.5) selected if the residues Ka/Ks confidence interval does not overlap neutral selection (Ka/Ks ≈ 1.0, fig. 1A; supplementary tables S1 and S2 and figs. S1–S4, Supplementary Material online). The evolution of *TYRO3* in primates has been dominated by a mixture of neutral and weakly purifying selection, with a higher degree of conservation present in the kinase domain (fig. 1A, supplementary fig. S2, Supplementary Material online). *AXL* is strongly conserved, with >90% of the gene displaying strong sequence conservation (fig. 1A, supplementary fig. S3, Supplementary Material online). In marked contrast, *MERTK* displays two large islands of strong positive selection (amino acids 1–21 and 518–532) interspaced by regions dominated by negative selection (fig. 1A, supplementary fig. S4, Supplementary Material online). Consistent with these observations, *AXL* and *TYRO3* have undergone a smaller degree of evolutionary divergence than *MERTK* during primate evolution, with *MERTK* displaying significant sequence divergence even in the Hominini clade (fig. 1B–D). At the whole-gene level TYRO3 and AXL display an evolutionary pattern consistent with genetic drift (Z-score ≈ 0); in marked contrast, *MERTK* shows a high degree of conservation between humans and more distant phylogenetic groups, becoming significantly less conserved when humans are compared with closer phylogenetic groups (fig. 1E, supplementary tables S3–S5, Supplementary Material online). Although the Z-scores comparing human to hominid and ape *MERTK* are consistent with drift, selecton analysis indicates that, in fact, different regions of *MERTK* have been under simultaneous positive and negative selection, thereby producing drift-like Z-scores (fig. 1A, supplementary fig. S4, Supplementary Material online).

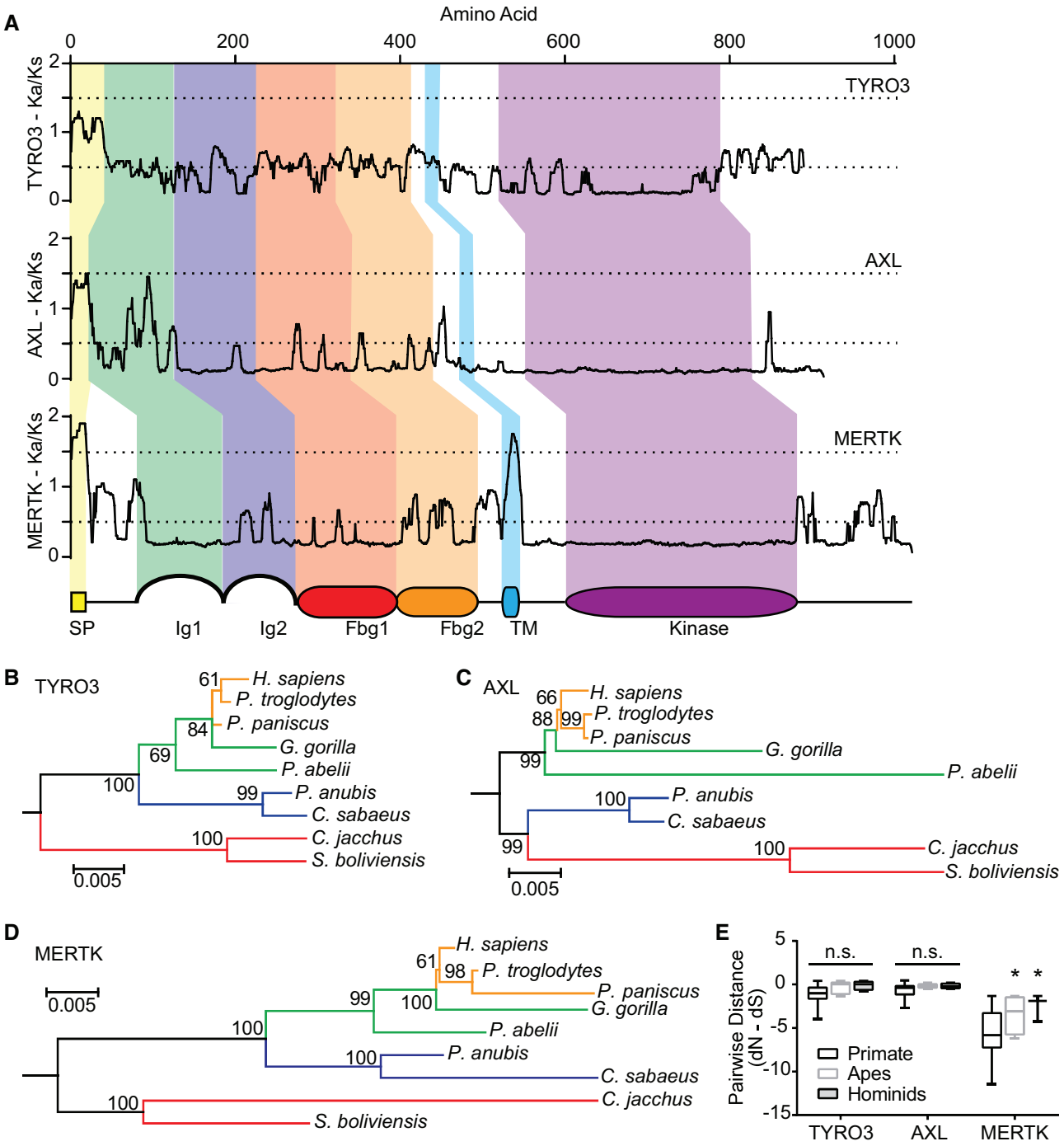

Fig. 1. Recent Evolution of *TYRO3*, *AXL*, and *MERTK*. (*A*) Identification of regions of positive and purifying selection by Ka/Ks analysis, averaged over ten neighboring amino acids. Ka/Ks > 1.5 indicate positive selection, Ka/Ks < 0.5 indicate purifying selection (horizontal dotted lines). Major structural domains are indicated by colored shading; a generalized domain diagram is illustrated at the bottom of the figure. SP = signal peptide, Ig = immunoglobulin domain, Fbg = fibrinogen-like domain, TM = transmembrane domain, Kinase = tyrosine kinase domain. (*B*–*D*) Maximum-likelihood evolutionary trees of TYRO3 (*B*), AXL (*C*), and MERTK (*D*) containing representative members of the hominini (orange), the apes (hominini plus green), old-world monkeys (blue) and new-world monkeys (red). Scales indicate the degree of evolutionary divergence, numbers at branch-points indicate bootstrap values. (*E*) Pairwise distances (Z-score) comparing the estimated number of synonymous substitutions per synonymous site (*d*S) and the number of nonsynonymous substitutions per nonsynonymous site (*d*N) between the human and primate *MERTK* grouped into clades containing all primate, all apes, and hominids. * = $P < 0.05$, n.s. = $P > 0.05$ compared with the primate-ancestral gene, 2-way ANOVA with Tukey Correction.

MERTK Sequence Changes Resulting from Positive Selection

The higher degree of divergence in *MERTK*, combined with the presence of two regions of positive selection, led us to further characterize the nature of these changes on the sequence, expression, and function of MERTK. The first positively selected region, comprising amino acids 1 to 21, contains the entirety of the MERTK signal peptide plus an additional residue following the signal peptide cleavage site. The second positively selected region contains the TMD bordered by 7 extracellular and 5 intracellular membrane-proximal residues. The amino acid sequences of the hominid-ancestral and primate-ancestral signal peptides were inferred using *MERTK* sequences from all available primate species and a maximum likelihood approach (see supplementary table S1, Supplementary Material online). Two mutations in the signal peptide arose in hominids; the first (G14C) resulted in an arginine-to-proline substitution (R5P) which reduced the polarity of the primate signal peptide (table 1), and the second (C69T) resulting in a synonymous threonine mutation (T23T) in a neutrally evolving region following the signal peptide cleavage site (fig. 2*A* and *B*). A third mutation arose in humans (A55C), which substituted an arginine for a serine (S20R) and restored the polarity of the human signal peptide to that of the primate-ancestral sequence (fig. 2*A* and *B* and table 1). The signal peptide of *MERTK* mRNA is highly GC-rich (75% GC), which can be indicative of the presence of non-B DNA motifs, which can form structures known to regulate gene expression at both the transcriptional and translational level (Emes and Yang 2008; Bansal et al. 2014). Analysis of the ancestral *MERTK* signal peptide for non-B motifs revealed that the human, ancestral-hominid, and ancestral-primate signal peptides contain a triplet GCT direct repeat (base pairs 20–29, fig. 2*C*), which can form slipped hairpin motifs, whereas the G14C mutation that arose in hominids produced a probable cruciform motif spanning base pairs 3–14 that was not present in the primate-ancestral sequence (fig. 2*C*). No SNPs are reported in 1000 genome databases for the sites containing the G14C, A55C, C69T mutations, suggesting these may be genetically fixed in humans (1000 Genomes Project Consortium et al. 2015).

INDELs have occurred in the *MERTK* TMD throughout primate evolution, including two insertions during the divergence of hominids (fig. 2*D*). These insertions lengthened the MERTK TMD from a 17-residue domain in the ancestral primate sequence to a 21-residue domain in the ancestral hominid sequence, increasing the hydrophobicity of the TMD (table 1). In addition, three point mutations arose in the human lineage. The first two (A1495G and T1560C) occurred in hominids, resulting in a threonine to alanine substitution (T499A) and a silent mutation (I521), respectively. The final mutation (G1552A) arose during the divergence of humans and substituted isoleucine for valine (V518I, fig. 2*D* and *E*). These mutations did not significantly affect the isoelectric point or hydrophobicity of the MERTK TMD (table 1). No SNPs are reported in 1000 genome databases for the sites containing the TMD insertions, whereas the V518I mutation is minimally polymorphic, with $<0.1\%$ of humans having the ancestral G1552 SNP, suggesting that most of these sites are genetically fixed in humans (1000 Genomes Project Consortium et al. 2015). No non-B motifs were identified in the MERTK TMD.

Decreased MERTK Expression via Signal Peptide Evolution

To determine if the evolution of the *MERTK* signal peptide altered MERTK expression or trafficking to the cell surface, we synthesized an optimized version of human *MERTK*, thus eliminating any effects of non-B motifs on our analyses (see supplementary fig. S5, Supplementary Material online). Next, amino acids 1–26 of the optimized *MERTK* construct were replaced with the equivalent portions of the human, reconstructed-hominid or reconstructed-primate *MERTK* signal peptide using Gibson assembly (Gibson et al. 2009). These constructs enabled comparisons of signal peptide efficacy in protein expression and trafficking, independent of any effects incurred by evolution elsewhere in *MERTK*. Ectopic expression of MERTK, using appropriate transfection controls and densitometric quantification of immunoblots, revealed a nearly 3-fold decrease in human MERTK expression relative to ancestral-primate MERTK (fig. 3*A* and *B*). To test if this decrease in expression is due to altered MERTK protein secretion, we measured the export of *de novo* synthesized MERTK from the Golgi to the cell surface using a cycloheximide-chase assay. No significant difference in MERTK export rates were observed amount the human, hominid-ancestral, and primate-ancestral constructs (fig. 3*C* and *D*). We also observed no significant difference in the half-life of the different MERTK constructs (fig. 3*E* and *F*). These findings indicate that the decreased human MERTK expression, compared with primate-ancestral expression, is not regulated at the protein level.

Compensatory Evolution of the MERTK Transmembrane Domain

The expansion of the TMD through the addition of leucines and isoleucines (fig. 2*E*) is suggestive of the evolution of a new interprotein interaction domain, such as those which promote receptor dimerization (Li et al. 2012). Protein modeling of the human, ancestral-hominid, and ancestral-primate TMDs predicted that all three TMD domains were helical, with the ancestral-primate transmembrane helix slightly shorter than the human and ancestral-hominid TMD domains (fig. 4*A* and *B*). Interestingly, the human and ancestral-hominid TMDs evolved two distinct features not present in the ancestral-primate TMD—first, a polar serine residue became incorporated into the human and ancestral-hominid helical domains, and second, additional hydrophobic residues (leucines and isoleucines) were added to the same face of the TMD in the human and ancestral-hominid sequences, forming a hydrophobic cluster (fig. 4*C*). Hydrophobic clusters are common motifs found in protein–protein interaction domains, leading us to investigate

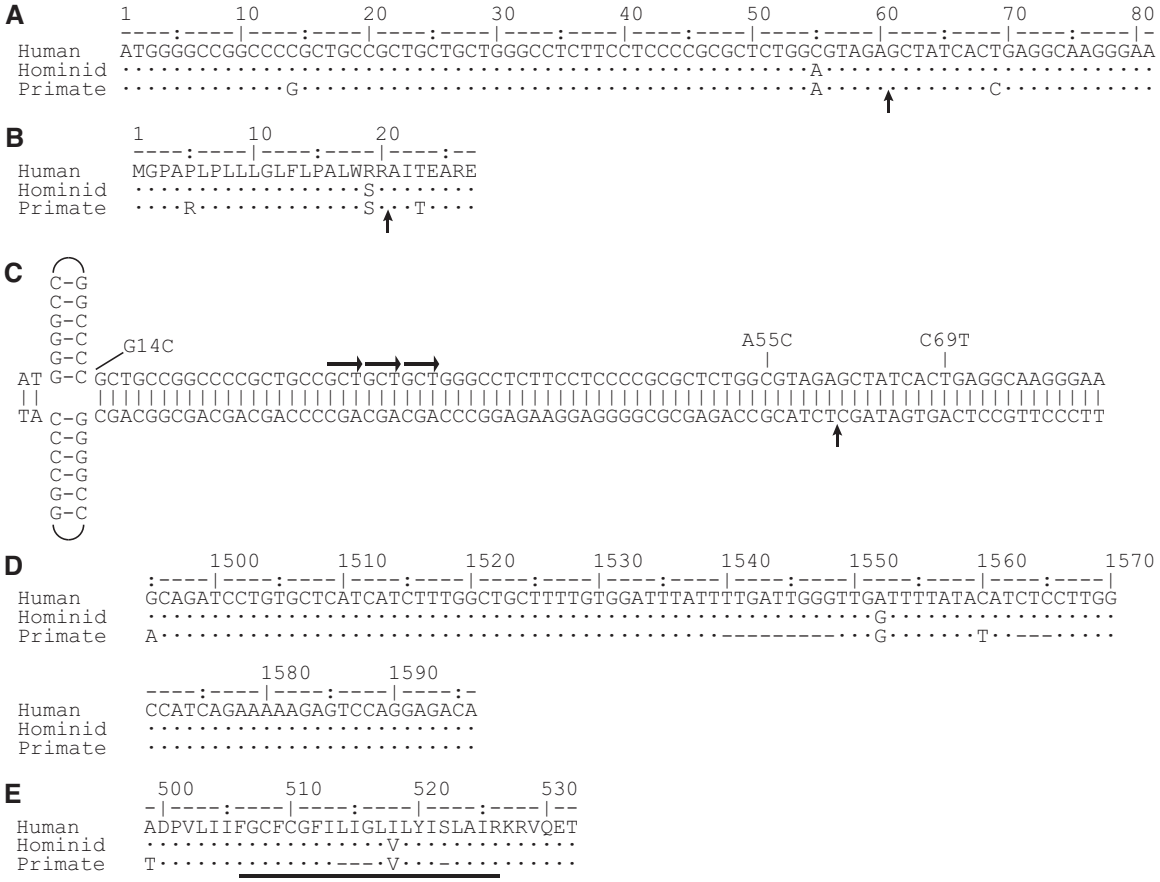

Fig. 2. Reconstruction of Recent Evolution in the *MERTK* Signal Peptide and Transmembrane Domain. (*A* and *B*) Alignments of the human, hominid-ancestral, and primate-ancestral signal peptide DNA (*A*) and protein (*B*) sequence. The signal peptide cleavage point is indicated by the vertical arrow. (*C*) Predicted non-B DNA structure and SNP's in the *MERTK* signal peptide. Tandem GCT repeats are indicated by horizontal arrows, the signal peptide cleavage point is indicated by the vertical arrow. (*D*–*E*) DNA (*D*) and protein (*E*) alignments of the human, hominid-ancestral and primate-ancestral TMD, and membrane-proximal regions. Horizontal line indicates the TMD. Ancestral sequences were inferred using a maximum-likelihood approach.

Table 1. Biochemical Characteristics of the Human, Hominid-Ancestral, and Primate-Ancestral MERTK Signal Peptide (Human Residues 1–27) and Transmembrane Domains (Human Residues 499–532).

Clade	Domain	pI[a]	Hydrophobicity[b]
Human	**Signal Peptide**	**10.61**	**0.51**
	Transmembrane	**8.92**	**1.38**
Hominid	**Signal Peptide**	**7.07**	**0.64**
	Transmembrane	**8.92**	**1.37**
Primate	**Signal Peptide**	**10.61**	**0.54**
	Transmembrane	**7.72**	**1.23**

[a]Mono-isotopic isoelectric point.
[b]Hydrophobicity index (Kyte and Doolittle 1982).

whether these changes to the TMD altered MERTK structuring on the cell surface.

To determine whether the changes to the MERTK TMD altered MERTK clustering, the TMD of the optimized human MERTK constructs described above were replaced with the equivalent portion of the human, ancestral-hominid, and ancestral-primate MERTK TMDs. The resulting Green Fluorescent Protein (GFP) fusion proteins were expressed in HeLa cells, imaged using super-resolution GSDM microscopy at a resolution of 20 nm, and MERTK self-clustering assessed by radial distribution analysis (Caetano et al. 2015). Ancestral-primate, ancestral-hominid, and human MERTK all formed micro-clusters on the plasmalamella (fig. 5*A*); however, the proportion of MERTK undergoing clustering increased approximately 4-fold in the human and ancestral-hominid sequences compared with ancestral-primate (fig. 5*B* and *C*). Ancestral-primate MERTK clusters averaged 20–40 nm in diameter, consistent with homodimers, whereas human and ancestral hominid MERTK formed clusters averaging 80–100 nm in diameter (fig. 5*B* and *D*). The corresponding signal peptides were then added to the TMD constructs, to recapitulate the impact of both areas of positive selection on MERTK function. Even though human MERTK was expressed at lower levels than primate-ancestral or hominid-ancestral MERTK (fig. 3*A*–*C*), MERTK-dependent binding of apoptotic cell mimics was consistent across all three forms of MERTK (fig. 5*E*). This lack of difference in ligand binding, despite differing levels of expression, suggests that the increased clustering of human and hominid-ancestral MERTK may act to compensate for lower expression through increased avidity. MERTK avidity was therefore quantified using a flow-based

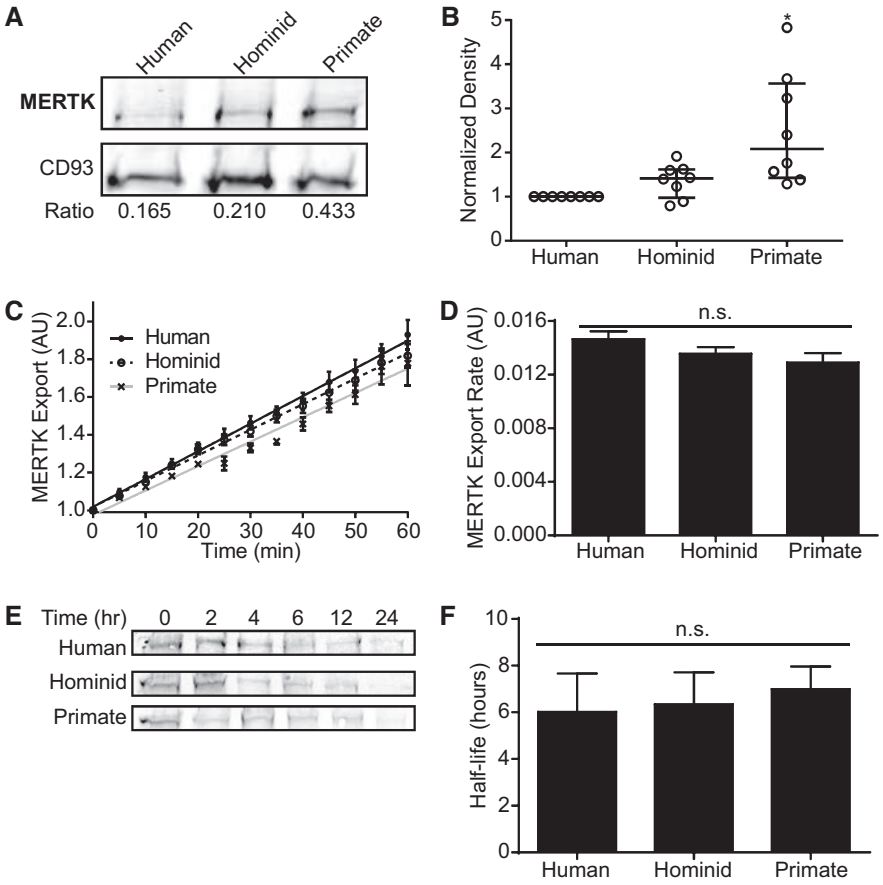

Fig. 3. Influence of MERTK Signal Peptide Evolution on Protein Processing and Expression Level. MERTK bearing a human, ancestral-hominid, or ancestral-primate signal peptide were expressed in HeLa cells and their secretion, total expression, and half-lives quantified. (*A* and *B*) Total MERTK expression as quantified by the ratio of MERTK expression to the expression of a transfection control under the control of the same promotor (CD93). (*A*) Representative immunoblot, (*B*) quantification of MERTK expression, normalized to CD93. (*C* and *D*) Secretion of *de novo* synthesized MERTK was quantified by saturation-labeling of cell-surface HA-MERTK-GFP with Cy3, followed by quantification of the GFP:Cy3 ratio with fluorescence microscopy, (*C*) change in GFP:Cy3 ratio, normalized to time 0, and (*D*) MERTK export rate, quantified as the slope of panel *A*. (*E* and *F*) Quantification of MERTK half-life, (*E*) representative immunoblot, and (*F*) calculated half-life. $n = 5–10$. n.s. $= P > 0.05$, * $= P < 0.05$, compared with Human, Kruskal–Wallis test with Dunn correction.

shear system, with human and hominid-ancestral MERTK binding much more strongly than primate-ancestral MERTK at all shear forces tested (fig. 5*F*). Consistent with this increase in binding being a product of increased affinity, the largest differences between human, hominid-ancestral, and primate-ancestral binding was observed in cells with lower MERTK expression levels, where the magnitude of the clustering-induced increase in local MERTK concentration is the greatest (fig. 5*G*). Interestingly, the ten amino-acid hydrophobic cluster in human *MERTK* which mediates this clustering is not present in any other vertebrate genes other than hominid *MERTK* orthologs (Clark et al. 2016), suggesting that this motif may be specific to MERTK-mediated interactions.

The evolution of lowered MERTK expression counterbalanced by increased avidity, the presence of positively-selected domains, and MERTKs known roles in mediating enveloped virus infection and immunomodulation (Best 2013; Bhattacharyya et al. 2013; Tsou et al. 2014; Dahlmann et al. 2015), indicates that this evolution of MERTK is likely a product of virus-driven antagonistic coevolution. Previous studies showed that enveloped viruses, including Ebola virus, can utilize MERTK for entry into macrophages and other MERTK-expressing cell types (Shimojima et al. 2006; Dahlmann et al. 2015). As such, we tested if cells expressing human MERTK bearing human, hominid-ancestral or primate-ancestral signal peptides and TMDs exhibited altered binding of enveloped Ebola virus-like particles (VLPs) containing both the matrix (VP40) and surface-exposed (glycoprotein) proteins of Ebola (Zaire). As shown in fig. 5*H*, cells expressing human or hominid-ancestral MERTK exhibited significantly lower particle binding than primate-ancestral MERTK, confirming that the reduced expression and increased clustering of hominid/human MERTK is sufficient to reduce viral parasitism of MERTK-expressing cells without compromising MERTK function.

Discussion

In this study, we have identified two areas of intense positive selection in the TAM receptor MERTK which arose during the evolution of humans from earlier primates. This selection

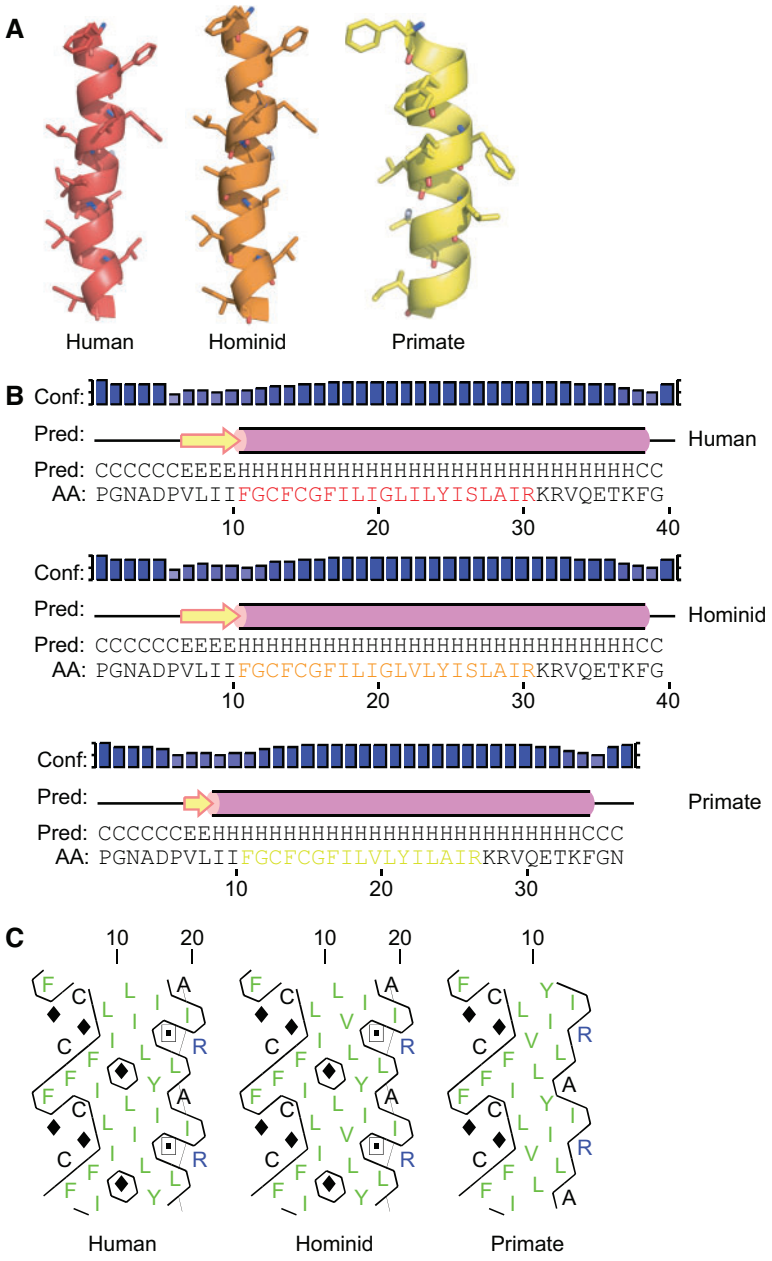

Fig. 4. Protein Modeling of MERTK Transmembrane Domain. Amino acids 506–533 of human MERTK and the equivalent portion of the ancestral-hominid and ancestral-primate MERTK sequences, containing the TMD plus 10 N-terminal and 10 C-terminal residues were subjected to protein structure predictive modeling. (*A*) Ribbon diagram of the predicted structure and length of the MERTK TMD. (*B*) Confidence of helical structure versus nonhelical structure prediction. (*C*) Hydrophobic cluster analysis projected onto a 2D model of the MERTK TMD. Hydrophobic clusters appear in boxes, nonhydrophobic residues are in diamonds.

occurred in the signal peptide and TMD, with the combined effect of lowering MERTK expression while maintaining normal MERTK efferocytic function through increased avidity. This pattern of evolution is consistent with pathogen-driven antagonistic coevolution (Williams et al. 2000; Sawyer et al. 2005; Paterson et al. 2010), and indeed, led to reduced binding of Ebola virus-like particles in cells expressing human versus ancestral forms of MERTK. Positive selection is a relatively rare occurrence in human evolution, and is most often observed in genes related to reproduction, olfaction, skin pigmentation or the immune system (Vallender and Lahn 2004; Bakewell et al. 2007; Williamson et al. 2007). In immune-related genes positive selection typically occurs in response to pathogens, often taking the form of antagonistic coevolution; however, the biological impact of these evolutionary changes in immune function remains poorly understood. As one example, Ortiz et al. identified a number of immune genes related to HIV-1 pathogenesis that had a higher median K_A/K_S value than control genes, but while in some cases this selection could be mapped to protein domains with a known function, the specific changes in gene function generated by these evolutionary events is unknown

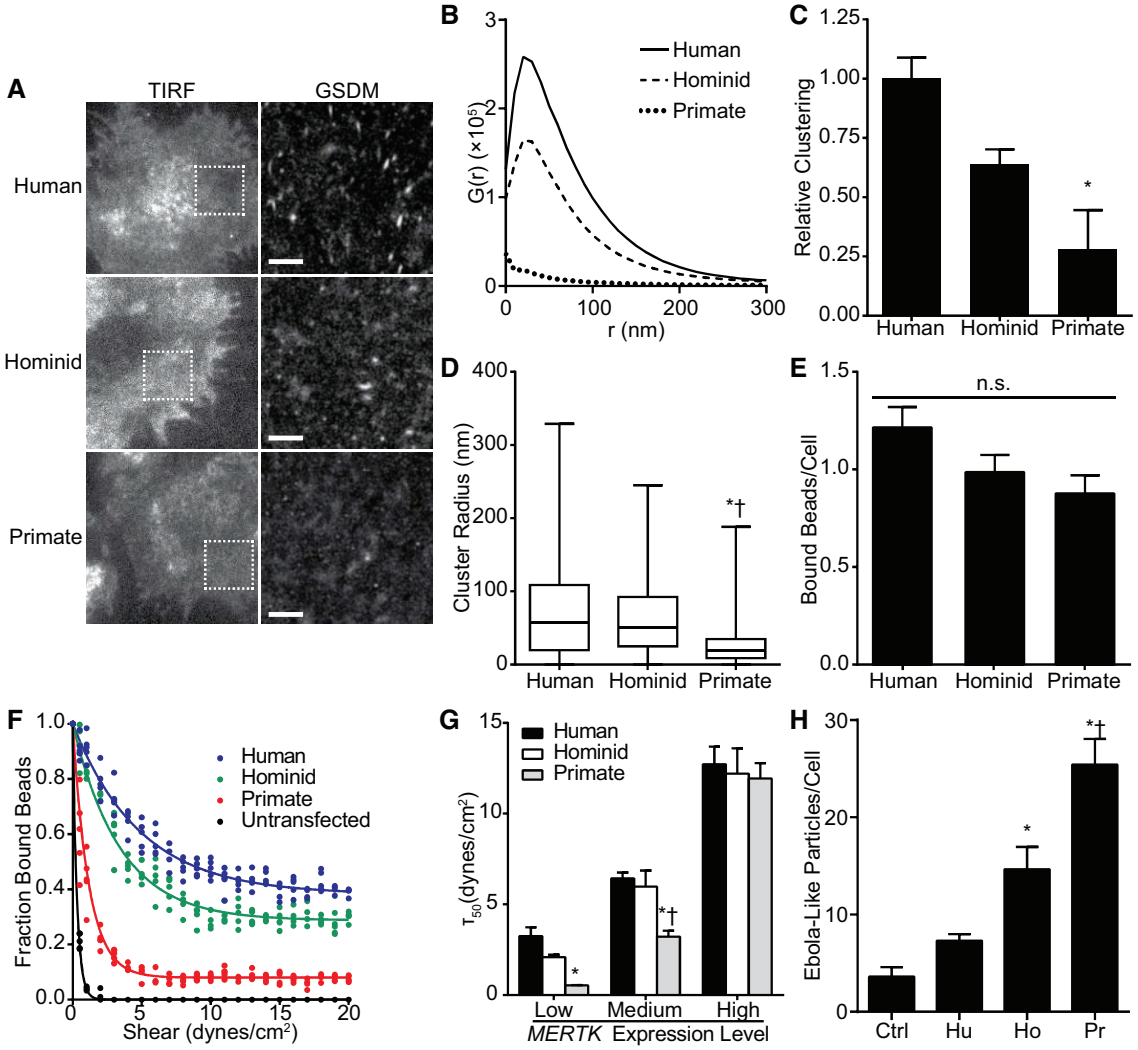

Fig. 5. Evolution in MERTK Clustering and Avidity Driven by Transmembrane Domain Evolution. HeLa cells transfected with constructs containing human *MERTK-GFP* modified to contain the hominid or ape ancestral TMD were quantified for MERTK self-clustering, avidity, and enveloped viral binding. (*A*) Total Internal Reflection Microscopy (TIRF) and super-resolution ground state microscopy images (GSDM) of MERTK TMD constructs in the basolateral membrane. Boxes in the TIRF image indicate the 5 × 5 μm^2 region shown in the GSDM image, scale bars are 1 μm. (*B*) Quantification of MERTK clustering by the radial distribution function G(r). (*C*) Clustering of MERTK TMD constructs, expressed as the area under the G(r) curve ± SEM, normalized to the degree of clustering observed in the primate-ancestral construct. (*D*) MERTK cluster radius, plotted as median ± interquartile range (whiskers = 5th/95th percentile). (*E*) Binding of apoptotic cell mimics by MERTK bearing human, hominid-ancestral or primate-ancestral TMDs. (*F*) Binding of apoptotic cell mimics by MERTK bearing human, hominid-ancestral or primate-ancestral TMDs at increasing shear stress. (*G*) Correlation between low-, medium-, and high-MERTK expression levels and the shear stress at which 50% of apoptotic cell mimics were retained on transfected cells. (*H*) Binding of Ebola VLPs to untransfected cells (Ctrl) or to cells expressing MERTK bearing Human (Hu), Hominid-ancestral (Ho) or Primate-ancestral (Pm) signal peptides, and TMDs. $n = 3$; * = $P < 0.05$ compared with Human, † compared with Hominid, n.s. = $P > 0.05$, ANOVA with Tukey correction.

(Ortiz et al. 2009). In our evolutionary analysis of the TAM receptors, we were able to ascribe specific changes in human MERTK biology to the evolutionary processes we identified, specifically linking the evolution of a non-B DNA motif within the signal peptide to a significant decrease in MERTK expression, and a corresponding compensatory increase in MERTK avidity driven by evolution of a new hydrophobic motif in the TMD. Both of these changes to MERTK's biological activity occurred via positive selection, indicative of antagonistic coevolution, and indeed, these changes to MERTK resulted in lowered binding of an enveloped virus to MERTK while maintaining normal efferocytic activity.

TAM receptors function predominantly as efferocytic receptors, enabling the recognition and phagocytosis of ACs through the binding of PtdSer exposed on the AC's plasma membrane (Ishimoto et al. 2000; Grommes et al. 2008). TAM receptors mediate a number of cellular responses upon engaging an apoptotic cell, including driving actin cytoskeleton reorganization in order to engulf the AC, and engagement of antiinflammatory signaling pathways to suppress immune responses. These two processes are central to the maintenance of homeostasis—by removing ACs TAM receptors prevent the inflammation and release of self-antigens which follows secondary necrosis of uncleared ACs, whereas

the induction of antiinflammatory signaling further acts to ensure the quiescence of immune cells within healthy tissues (Rothlin et al. 2007; Li et al. 2013; Zagórska et al. 2014; Grabiec and Hussell 2016). These characteristics of TAM receptors has led to their targeting by both cancer and viruses for immune evasion. TAM receptor-expressing cancer cells sequester tumor-derived antigens through engulfment of dying tumor cells, thereby limiting tumor immunogenicity, whereas simultaneously dampening proinflammatory cytokine production via TAM-dependent SOCS1 and SOCS3 signaling (Bosurgi et al. 2013; Nguyen et al. 2014; Stanford et al. 2014; Kimani et al. 2016). Enveloped viruses engage TAM receptors by incorporating PtdSer in their lipid envelope. Some viruses engage TAM receptors strictly for immunomodulation, through inhibiting the effect of the interferon antiviral response through upregulation of the interferon-receptor inhibiting SOCS1 and SOCS3 proteins (Bhattacharyya et al. 2013; Shibata et al. 2014; Read et al. 2015). Other viruses, such as flaviviruses and some retroviruses, utilize TAM receptors to gain entry into target cells. Indeed, MERTK-deficient human macrophages are refractory to infection by Ebola and Marburg viruses, whereas MERTK-deficient mouse macrophages have reduced rates of infection by Murine Leukemia Virus (Shimojima et al. 2006; Bhattacharyya et al. 2013; Dahlmann et al. 2015). Although all three TAM receptors have similar antiinflammatory and efferocytic capabilities, MERTK appears to be a more critical member of the TAM receptor family. Indeed, MERTK deficient animals are hyperinflammatory in response to toll-like receptor ligands (Lee et al. 2012), are susceptible to atherosclerosis (Thorp et al. 2008; Wan et al. 2013), develop autoimmunity (Wallet et al. 2008; Zizzo et al. 2012) and develop retinitis pigmentosa (Duncan et al. 2003)—phenotypes similar to that observed in TAM triple-knockout mice (Li et al. 2013). In contrast, AXL and TYRO3 knockouts are phenotypically normal, and neither autoimmunity or inflammatory diseases such as atherosclerosis have been reported in these animals (Lu et al. 1999; Subramanian et al. 2016). In humans, SNPs in MERTK are associated with retinal dystrophy, multiple sclerosis, and atherosclerosis, whereas SNPs in AXL and TYRO3 have no reported clinical associations (Brea-Fernández et al. 2008; Hurtado et al. 2010; Ma et al. 2011; Binder et al. 2016; Cavalli et al. 2016). Although the reason for this preferential requirement for MERTK remains unknown, the relative importance of MERTK in mammalian biology may explain why it, and not TYRO3 or AXL, has been subject to intense selection during the divergence of humans from primates.

The positive selection of the MERTK signal peptide is anomalous in protein evolution. Signal peptides are relatively free to evolve so long as they continue to meet minimal biochemical attributes—that is, polar or neutral amino acids surrounding a somewhat hydrophobic core (Li et al. 2009; Gralle and Pääbo 2011). These minimal requirements permit signal peptides to evolve at a faster rate than the mature peptide, although an overall trend of moderate conservation tends to be observed ($K_A/K_S \approx 0.63$) (Williams et al. 2000). The signal peptides of a few mammalian immune-related genes have been shown to contain positive selection, specifically IFN-γ, CTLA-4, and the small cytokine A11 (Williams et al. 2000; Wang et al. 2014), but the biological impact of this selection remains unexplored. Outside of mammals there have been a some reports of positive selection in signal peptides—for example in mollusk and gastropod sperm proteins, where selection is hypothesized to have played a role in speciation through an uncharacterized mechanism (Lee et al. 1995; Hellberg et al. 2000). Our investigation into the biological changes incurred by recent evolution in MERTK revealed a significant reduction in protein expression which we propose occurred in response to parasitism of MERTK by viral pathogens. Indeed, decreased viral receptor expression has been shown to reduce viral infection; for example, reducing expression of the HIV coreceptor CCR5 decreases the susceptibility of cells to HIV infection (Heredia et al. 2007). The molecular mechanism underlying the decrease in MERTK expression is not known; however, we showed that this decrease is not likely due to reduced export of newly synthesized MERTK or due to increased protein turnover. It is possible that the decrease in MERTK expression we observed occurs through formation of a non-B DNA cruciform motif, located within base pairs 3–15 of the MERTK coding region, creating a hairpin structure on both DNA strands (Kim et al. 1998; Brázda et al. 2011). Cruciform structures are known to inhibit DNA transcription through steric hindrance of RNA polymerase, and translation of mRNA by hindering ribosome function (Perros et al. 1994). Future experiments are necessary to determine if these possibilities account for the decreased MERTK expression we observed.

As with the signal peptide, the presence of positively selected residues in the MERTK TMD is anomalous compared with typical patterns of TMD evolution. The hydrophobic helical core of a TMD is normally highly conserved, with more modest conservation observed in lipid-exposed regions and oligomerizing surfaces (Stevens and Arkin 2001; Dean et al. 2002; Leabman et al. 2003; Mokrab et al. 2010). Although quite rare, positive selection has been observed in TMDs among the G-protein coupled receptors responsible for olfaction, where positive selection alters the ligand binding site formed by the TMDs (Singer et al. 1996; Steiger et al. 2010). This process is not likely responsible for the evolution of the MERTK TMD, as TAM ligand recognition occurs in the extracellular tandem immunoglobulin repeats (Sasaki et al. 2006). TMD evolution can also alter interprotein interactions through the creation or elimination of intermembrane interaction motifs. As one example, tetherin, an inhibitor of viral budding, has undergone significant positive selection within its TMD—presumably in response to selective pressure from lentiviruses. Coevolution in the lentiviral Vpu protein, which inactivates tetherin, has led to interaction motifs in Vpu that engage these unique motifs in the tetherin TMD, a protein–protein interaction which defines the species specificity of many lentiviruses (McNatt et al. 2009). The pattern of TMD evolution we observed in MERTK is consistent with the formation of a new leucine-zipper-like motif, and consistent with this, we observed an increase in MERTK cluster size as this motif evolved from primates to humans. Increased

protein clustering is often an indication of an increase in avidity (van Kooyk et al. 1999), and indeed, we observed a significant increase in the avidity of human versus primate MERTK. This increase in avidity may compensate for the decreased expression levels of human MERTK due to signal peptide evolution, thereby maintaining normal MERTK functional capacity despite the dramatically lower expression level.

Antagonistic coevolution is a common mechanism of host-pathogen coevolution. In humans, antagonistic coevolution is most often observed in immune-related genes; an unsurprising finding given the central role of the immune system in mediating host-pathogen interactions (Sabeti et al. 2007; McNatt et al. 2009). Antagonistic coevolution—also known as the Red Queen hypothesis—creates an arms race in which the pathogen or host briefly gains an advantage through adaptive evolution, only to lose that advantage when the competing species evolves a compensatory trait (Van Valen 1973; Nordbotten and Stenseth 2016). The selective pressure applied to both species has the dual impacts of increasing the rate at which deleterious mutations are purged and beneficial mutations are acquired, greatly accelerating molecular evolution (Buckling et al. 2006; Paterson et al. 2010). For example, the rate of genetic divergence of the Φ2 bacteriophage doubled when both Φ2 and the host species *Pseudomonas fluorescens* were serially cultured together—thus allowing for coevolution—versus when Φ2 was serially propagated using isogenic cultures of *P. fluorescens* (Paterson et al. 2010). This accelerated evolution was not merely a nonspecific accumulation of mutations, but rather coevolved Φ2 accumulated nonsynonymous mutations preferentially over synonymous mutations—indicative of positive selection, and representing the same evolutionary pattern we observed in *MERTK*. Indeed, hominids acquired an initial set of mutations which acted to partially decrease MERTK expression and partially enhance clustering, with additional mutations arising in the human lineage that further decreased expression and further enhanced clustering—a pattern of step-wise evolution consistent with the arms-race nature of antagonistic coevolution. It is tempting to hypothesize that retroviruses are responsible for the antagonistic coevolution of *MERTK*, as these viruses can parasitize MERTK and are known to have played other important roles in the evolution of primates, hominids, and humans, but it is unlikely that the causative agent for this evolution will ever be identified. (Dawkins et al. 1999; Hughes and Coffin 2001; Yohn et al. 2005; Doxiadis et al. 2008; Dahlmann et al. 2015).

In conclusion, we discovered evidence for strong positive selection in *MERTK*'s signal peptide and transmembrane domain, which appear to be a form of antagonistic coevolution with enveloped viruses that reduces the availability of MERTK for viral binding, whereas maintaining normal MERTK function. This strong evolutionary response highlights *MERTK*'s importance as a critical mediator of homeostasis and as a virion binding receptor, and illustrates the how compensatory evolution can act to overcome viral pathogenesis.

Materials and Methods

Materials

COS-7 cells were a gift from Dr. Sergio Grinstein (Hospital for Sick Children, Toronto), and DH5a *Escherichia coli* were gifts from Dr. John McCormick (University of Western Ontario). Roswell Park Memorial (RPMI), Dulbecco's Modified Eagle Medium (DMEM), Trypsin-EDTA, and Fetal Bovine Serum (FBS) were purchased from Wisent (Saint-Jean-Baptiste, Canada). #1.5 thickness round cover slips and 16% paraformaldehyde (PFA) were purchased from Electron Microscopy Supplies (Hatfield, Pennsylvania). Cysteamine, L-Cysteine, DTT, cycloheximide, dexamethosome, and rat anti-HA (3F10) were purchased from Sigma-Aldrich (Oakville, Canada). GenJet Plus was purchased from Frogga Bio (North York, Canada). Hoechst, permafluor, protease inhibitor cocktail, T4 DNA ligase, and Phusion DNA polymerase were purchased from Thermo Scientific (Mississauga, Canada). Silica beads were purchased from Bangs Laboratories (Fishers, Indiana), and lipids were purchased from Avanti Polar Lipids, Inc. (Alabaster, Alabama). Recombinant human GAS6 and all restriction enzymes were purchased from R&D (Minneapolis, MN). Mouse anti-HA (12CA5) was purchased from Santa Cruz (Dallas, Texas). Florescent secondary antibodies were purchased from Life Technologies (Burlington, Canada). All other chemicals were purchased from Canada BioShop (Mississauga, Canada). Matlab software was purchased from MathWorks (Natick, Massachusetts). Prism software was purchased from Graphpad (La Jolla, California). Mega6 Software (Tamura et al. 2013) was downloaded from http://www.megasoftware.net (last accessed March 10, 2017).

Generation of Phylogenic Trees

All phylogenetic and molecular evolutionary analyses were conducted using MEGA version 6 (Tamura et al. 2013). Briefly, primate *MERTK* sequences were retrieved from the NCBI database and coding sequence alignments for mammals and primates were generated by *Muscle* using default parameters (see supplementary table S1, Supplementary Material online). For phylogenetic analysis, Bayesian (BIC) and Akaike information criterion (AIC) scores for each nucleotide substitution model were compared with determine the model used for alignments. Phylogenetic analyses of aligned sequences were performed across all reading frames using maximum-likelihood with bootstrapping using the GTR model for *MERTK* sequence analysis, whereas the *AXL* and *TYRO3* phylogenetic analyses used the T92 and TN93 selection models, respectively, both with gamma distribution. The phylogenetic trees were annotated using EvolView. Human SNP data was acquired from the 1000 Genome Project (1000 Genomes Project Consortium et al. 2015).

Selection Analysis

Unaligned TAM primate sequences were imported into the Selecton online sever (http://selecton.tau.ac.il/; last accessed March 10, 2017). For each analysis the *Homo sapiens* sequence was selected as a reference sequence, and previously

generated phylogenetic trees used as alignment guides. Selection analyses were performed using the Mechanistic Empirical Combination Model (MEC) using eight distribution categories and the JTT amino-acid matrix (Doron-Faigenboim et al. 2005). As a test of significance, MEC likelihood and AIC scores were compared against the M8a model, with lower MEC AIC scores indicating significance. Additionally, selection analysis was performed using the M5 model, with AIC scores compared with the M7 model as a test of significance. Further selection analysis used the M5 model, comparing AIC scores with the M7 model. A comparison between the MEC/M8a and M5/M7 AIC scores confirmed MEC as the model of best fit by maximum-likelihood. Amino acid positions were scored for significance using Ka/Ks values and confidence intervals (CI) generated by Selecton. Ka/Ks scores >1.5 with CI lower bounds >1 were considered strong evidence of positive selection, whereas those with a CI lower bound of <1 were considered a possible indication of positive selection. Similarly, Ka/Ks scores of <0.5 with a CI upper bound <1 were considered strong evidence for purifying selection, whereas those with a CI upper bound >1 indicated possible purifying selection. Amino acid positions with Ka/Ks values close to 1.0 or those with large CIs where counted as showing no evidence of selection. Selecton data were then imported into Matlab and a custom-written script used to calculate regional Ka/Ks values by averaging the ten neighboring residues.

Prediction of Ancestral MERTK Sequences and Hydrophobicity and Isoelectric Point Analysis

Reconstruction of the ancestral Hominidae and Primate *MERTK* sequences were performed using Mega6 (Tamura et al. 2013). Nucleotide alignments and phylogenic trees of the Hominidae and Primate *MERTK* sequences, generated above, were imported into Mega6 and the ancestral sequences predicted a maximum-likelihood approach and the K2 evolutionary model. To analyze any biochemical changes in the reconstructed primate and hominid-ancestral MERTK signal peptides and TMDs, the amino acid sequences were imported into ExPASy ProtScale and Compute PI/Mw and hydrophobicity and isoelectric points calculated (https://www.expasy.org/; last accessed March 10, 2017).

MERTK Synthesis and Mutagenesis

As conventional cloning of human *MERTK* is not possible due to the presence of multiple motifs recognized by bacteria as recombination and phage integration sites, combined with an unusually high G/C content (Healy et al. 2016), we used the OptimumGene codon-optimization algorithm (GenScript) to remove secondary DNA structure and reduce GC content (see supplementary fig. S5, Supplementary Material online), and had the gene synthesized and subcloned into pcDNA3.1(+). An extracellular HA tag was added by linearizing the codon-optimized *MERTK* vector using the HA-FWD/HA-REV 5′ phosphorylated primers (see supplementary fig. S6, Supplementary Material online). PCR was conducted using Phusion DNA polymerase, 36 cycles with an annealing temperature of 63 °C and 8 min elongation at 72 °C. The PCR product was treated with DpnI at 37 °C for 1 h to degrade the template and gel purified using a 1% TAE/agarose gel and PCR purification kit. The purified linearized construct was then recircularized with T4 DNA ligase, transformed into DH5α *E. coli*, selected on LB agar + 100 μg/ml ampicillin, and insertion of the HA tag was confirmed by DNA sequencing. This HA-tagged vector and Gibson assembly were used for assembly of all subsequent *MERTK* constructs (Gibson et al. 2009). Briefly, the signal peptide and TMDs were replaced by linearizing the *HA-MERTK* construct by PCR using primers flanking the signal peptide (SigPep-FWD/SigPep-FWD) or TMD (TM-FWD/TM-REV, supplementary fig. S6, Supplementary Material online), using the same PCR cycle and purification protocol as above. The linearized vector was then mixed at a 1:5 molar ratio of vector:insert in a Gibson assembly master mix with synthesized double-stranded DNA constructs containing 20 bp regions of homology flanking the signal peptide (CD8α-SigPep, Human-SigPep, Hominid-SigPep, Primate-SigPep) or TMD (Hominid-TM or Primate-TM) sequence (see supplementary fig. S6, Supplementary Material online). The reaction was incubated at 50 °C for 30 min, then transformed into DH5α *E. coli* and positive clones identified as described above. Where GFP-tagged version of the vector were required, the constructs generated above were subcloned into pEGFP-N1 by PCR amplifying the modified MERTK gene with the SC-GFP-FWD/SC-GFP-REV primers using Phusion polymerase, 45 cycles, 63 °C annealing temperature and a 2 min elongation at 72 °C. The resulting PCR product was gel purified as above, and inserted into pEGFP-N1 by digesting the PCR product and vector with HindIII and AgeI and ligating the fragments together using T4 DNA ligase. mCherry-tagged constructs were generated by HindIII and AgeI subcloning of the pEGFP-N1 vectors created above.

Cell Culture and Transfection

HeLa cells were maintained in RPMI plus 10% FBS. Cells were split upon reaching 80% confluency by washing once with phosphate buffered saline (PBS: 0.9% NaCl, 10 mM Na_2HPO4, 2 mM KH_2PO_4, pH 7.4) followed by a 5 min incubation in trypsin-EDTA and resuspension in RPMI + 10% FBS. For imaging, #1.5 thickness 18 mm diameter coverslips were first rinsed in 100% ethanol, deproteinated for ~12 h in 1 M HCl at 50–60 °C with intermittent agitation, rinsed with 100% ethanol and dried. The coverslips were then placed into the wells of a 12-well tissue culture plate, 1 ml of RPMI + 10% FBS added, and 100 μl of the HeLa cell suspension added drop-wise to each well. 12 to 24 h later the cells were transfected with the desired construct following manufacturers protocols. Briefly, for each well two tubes of 38 μl serum-free DMEM were prepared and 1 μg of DNA added to one tube and 2 μl of GenJet Plus added to the second tube. Both tubes were vortexed briefly, the contents combined, and the mixture incubated for 10 min. The DNA:GenJet Plus complexes were then added drop-wise to the well and incubated 18–24 h.

Protein Trafficking Assay

HeLa cells were seeded onto μ-Slide 8 wells with a glass bottom and transfected at 80% confluency using Fugene HD at 2:0.75 transfection reagent to DNA (μl:μg) according to manufacturer's protocol. Transfected cells were washed three times using 10 °C PBS and incubated with 1:100 mouse anti-HA in serum-free RPMI for 20 min at 10 °C to label surface MERTK. Cells were washed three times using 10 °C PBS and incubated with 50 μg/ml cycloheximide in serum-free RPMI with 1:500 donkey antimouse 647 for 20 min at 10 °C. Cells were washed 3 times in 10 °C PBS and subsequently imaged in 37 °C serum-free RPMI with 50 μg/ml cycloheximide. The wells were placed onto a heated/CO_2 perfused live-cell piezoelectric stage of a Leica DMI6000B microscope equipped with a heated/CO2 perfused live-cell stage, Leica LAS-X software, a Photonics Evolve 2 EM-CCD camera, and a 63×/1.40NA objective lens. The position of 10–15 cells were marked using the stage controller and time-lapse videos of MERTK membrane trafficking captured (5 min/frame, 60 min duration). The plasmalamella of each cell was identified by the 647 staining (e.g., cell-surface MERTK). This mask was then applied to the GFP channel (total MERTK) and trafficking quantified as the rate of increase in GFP intensity within the 647 mask relative to the initial time point.

Protein Expression and Half-Life Assay

For protein expression assays, HeLa cells were transfected with 1 μg of a 1:30 mixture of the desired *MERTK* construct and HA-tagged *CD93*. 18 h after transfection the cells were lysed using Lammellis buffer (0.1% 2-Mercaptoethanol, 0.0005% Bromophenol blue, 10% glycerol, 2% SDS, 63 mM Tris–HCl, pH 6.8) plus protease inhibitor cocktail. For half-life assays HeLa cells were transfected with 1 μg of the desired MERTK construct; 18 h after transfection cells were treated with 50 μg/ml cycloheximide and lysed as above at the indicated time points. Samples were boiled for 5 min, cooled, and separated using a 10% SDS-PAGE gel at 150 V for 2 h. Samples were transferred to nitrocellulose membranes over 2 h at 80V, the membrane blocked with TBST (137 mM NaCl, 2.7 mM KCl, 19 mM Tris–HCl, 0.1% Tween-20, pH 7.4) plus 5% skim milk powder overnight at 4 °C. The blots were then incubated with 1:1000 rat-anti-HA in TBST + 5% skim milk powder for 2 h, washed 3 × 10 min with TBST, incubated with 1:15,000 Alexa800-lableled donkey-anti-rat in TBST + 5% skim milk powder, and washed a final 3 × 10 min with TBST. Blots were imaged using a Licore Odyssey Model 9120, and MERTK protein expression quantified as the ratio between the HA-CD93 and MERTK protein bands.

Protein Modeling

The TMDs of human hominid-ancestral and primate-ancestral MERTK were modeled by submitting amino acids 506–533 of human MERTK and the equivalent region of the reconstructed ancestral-hominid and ancestral-primate MERTK sequences to the Phyre2 web portal (Kelley et al. 2015), and the resulting images generated in PyMOL Molecular Graphics System, Version 1.8 (Schrödinger, LLC). Hydrophobic cluster identification of the regions identified as helical in the above sequences were then submitted to the HCA 1.0.2 server (http://mobyle.rpbs.univ-paris-diderot.fr; last accessed March 10, 2017) for identification of hydrophobic clusters as per the method of Gaboriaud et al. (1987).

Clustering Assay

Clustering of GFP-tagged MERTK was quantified using super-resolution Ground-State Depletion Microscopy. HeLa cells were transfected with GFP-tagged MERTK and fixed for 20 min at room temperature using 4% paraformaldehyde in PBS. The cells were washed three times in PBS and then permeabilized using PBS + 5% BSA and 0.01% saponin. The fixed and permeabilized samples were then mounted on depression slides with the depressions filled with imaging buffer (PBS + 100 mM Cysteamine). Once mounted the coverslips were sealed using Twinsil and mounted on a Leica SR GSD microscope equipped with a 100×/1.43 NA TIRF objective, plus an addition 1.6× optical magnifier for a total of 160× magnification, 125–250 mW imaging lasers (488, 555, and 647 nm) and a 30 mW backpumping laser (405 nm). Using total internal reflection mode, the GFP color channel was subjected to a depletion period where the sample was excited at maximum intensity until <120 active fluorophores were present in each image. The laser intensity was then reduced to 30–60% of maximum and the sample imaged at 100 fps for a minimum of 30,000 frames with the backpumping laser intensity increased over time to maintain an optimal number of active fluorophores/frame. The resulting molecule position files were exported, and to ensure equal sampling of all images, filtered to remove any molecule detections with a precession of more than 20 nm and resampled to an autocorrelation of 0.990 (Caetano et al. 2015). Four cells per condition were imaged in each experiment. Self-clustering was assessed using the radial distribution function, using our custom-written Matlab software for analysis (Heit et al. 2013; Caetano et al. 2015).

Binding Assay

MERTK-mediated efferocytosis was quantified as per our published protocols (Evans et al. 2017). Briefly, COS-7 cells were seeded onto 18 mm circular #1.5 thickness glass coverslips placed into the wells of a 12-well tissue culture and transfected with MERTK-GFP constructs bearing human, reconstructed-hominid and reconstructed-primate TMDs once cells reached 80% confluency, using GenJet transfection reagent as described above. 48 h later 10 μl of 3 μm diameter silica beads were combined with 145 μl of phosphatidylcholine, 114 μl PtdSer, and 4 μl of biotinylated-phosphatidylethanolamine. Beads were dried using nitrogen gas, resuspended in 500 μl PBS, centrifuged for 1 min at 4,500 × g, and washed twice in 500 μl of PBS. Beads were resuspended in 200 μl of PBS and 3 μl of bead solution per condition was opsonized with 4 nmol of GAS6 by rotation for 12 h at 4 °C. Solution was centrifuged for 1 min at 4,500 × g and washed three times in PBS and resuspended in 1 ml of serum-free RPMI per condition. 2×10^5 beads were then added per well, the tissue culture plates spun at 150 g for 1 min to force the beads into contact with the cells, and

the samples incubated for 60 min in a 37 °C/5% CO_2 incubator. The samples were then rinsed vigorously with PBS to remove any unbound beads, the cells fixed with 4% PFA in PBS for 20 min at room temperature, washed an additional three times in PBS, and the coverslips mounted onto slides with Permafluor. The slides were then imaged on the Leica DMI6000B microscope described above, using a 40×/1.25NA objective and the number of bound beads per transfected cell quantified, with at least 30 cells/condition imaged in each experiment.

MERTK Avidity Quantification

HeLa cells were cultured in 12-well plates and transfected as described above with human MERTK-GFP bearing human, reconstructed hominid-ancestral or reconstructed primate-ancestral TMDs. 24 h after transfection the cells were trypsinized with 300 µl of trypsin-EDTA followed by suspension in 1 ml of RPMI + 10% FBS and the suspended cells pelleted by a 300 × g/1 min centrifugation. The cell pellet was resuspended in 250 µl of RPMI + 10% FBS, 120 µl of the cell suspension placed into a channel of an Ibidi µSlide-VI, and the chamber incubated an additional 24 h. After 24 h the media in the chamber was replaced with 120 µl RPMI + 10% FBS containing 5×10^4 GAS6-opsonized PtdSer beads, as prepared above. The beads were incubated with the cells for 10 min, after which point the chamber was mounted on a Leica DMI6000B microscope using the 40× objective, and the chamber attached to a syringe pump in draw mode and to a reservoir of RPMI + 10% FBS at 37 °C. A 3 × 3 field of view area was selected for imaging, and a 3 × 3 tiled imaged captured of the DIC and GFP channels. Next, 30 s of shear applied at 0.5 dynes/cm^2 (0.388 ml/min), the flow stopped, and a DIC image captured of the same region. This shear and imaging process was then repeated for 1–20 dynes/cm^2, in 1 dyne/cm^2 increments (flow rates of 0.775–15.51 ml/min), with DIC images of the same area captured after each period of shear. The resulting GFP image was used to identify MERTK expressing and nonexpressing cells, and the number of beads bound to each cell at each increment of shear recorded. To assess the impact of MERTK expression level on bead binding, MERTK cells from this dataset were further segregated into quartiles based on their integrated MERTK fluorescence, with the lower-most quartile of cells removed from the analysis due to the difficulty of differentiating between weakly transfected cells and the background fluorescence of nontransfected cells. The avidity of the remaining three groups was then quantified as the shear rate at which 50% of beads remained bound to the cells (τ_{50}).

Viral Binding Assay

Ebola (Zaire) VP40-GFP and Ebola (Zaire) glycoprotein (GP)-derived noninfectious enveloped VLPs were generated by cotransfecting 293T cells with plasmids encoding VP40-GFP and GP constructs at a ratio of 1:1 using LipoD (Noda et al. 2002; Watanabe et al. 2004). Forty-eight h' posttransfection, supernatant containing Ebola VLPs was collected and clarified at 2,000 × g for 15 min. The same lot of freshly generated VLPs was used for all experiments to ensure equal viral loading. HeLa cells, transfected with human MERTK-mCherry bearing matched human, hominid or primate signal peptides, and TMDs, were cocultured with equivalent volumes of Ebola VLP-containing media for 1 h, washed 3× with PBS to remove unbound VLPs, and imaged at 112× magnification using the Leica DMI6000B microscope described above. Images from several fields of view were exported as TIFFs. Individual cell-bound VLPs were enumerated by mapping a Gaussian curve to the diffraction-limited GFP spot created by each VLP, using our previously published super-resolution single particle analysis software (Caetano et al. 2015; Goiko et al. 2016). The mCherry signal was used to differentiate MERTK-expressing and nonexpressing cells.

Statistical Analysis

Averaged selection values were calculated by importing selecton results into Matlab and using custom-written scripts to calculate a regional-average at each amino acid position ± 5 amino acids. All graphing and statistical analysis was performed in Graphpad Prism.

Supplementary Material

Supplementary data are available at *Molecular Biology and Evolution* online.

Acknowledgments

This study was funded by Canadian Institutes of Health Research Operating Grants MOP-123419 to B.H., HBF134179 and HBF137693 to S.B.D., and MOP-286719 to J.D.D.; by Natural Sciences and Engineering Research Counsel of Canada Discovery Grants 418194 to B.H., 386404 to S.B.D. and 435677 to J.D.D.; and by an Ontario Ministry of Research and Innovation Early Research Award to B.H. The funding agencies had no role in study design, data collection and analysis, decision to publish, or preparation of the manuscript.

References

1000 Genomes Project Consortium, Auton A, Brooks LD, Durbin RM, Garrison EP, Kang HM, Korbel JO, Marchini JL, McCarthy S, McVean GA, et al. 2015. A global reference for human genetic variation. *Nature* 526:68–74.

Bakewell M. a, Shi P, Zhang J. 2007. More genes underwent positive selection in chimpanzee evolution than in human evolution. *Proc Natl Acad Sci U S A*. 104:7489–7494.

Bansal M, Kumar A, Yella VR. 2014. Role of DNA sequence based structural features of promoters in transcription initiation and gene expression. *Curr Opin Struct Biol*. 25:77–85.

Best SM. 2013. Viruses play dead to TAMe interferon responses. *Cell Host Microbe* 14:117–118.

Bhattacharyya S, Zagórska A, Lew ED, Shrestha B, Rothlin CV, Naughton J, Diamond MS, Lemke G, Young JAT. 2013. Enveloped viruses disable innate immune responses in dendritic cells by direct activation of TAM receptors. *Cell Host Microbe* 14:136–147.

Binder MD, Fox AD, Merlo D, Johnson LJ, Giuffrida L, Calvert SE, Akkermann R, Ma GZM, Perera AA, Gresle MM, et al. 2016. Common and low frequency variants in MERTK are independently associated with multiple sclerosis susceptibility with discordant association dependent upon HLA-DRB1*15:01 status. *PLoS Genet*. 12:e1005853.

Bosurgi L, Bernink JH, Delgado Cuevas V, Gagliani N, Joannas L, Schmid ET, Booth CJ, Ghosh S, Rothlin CV. 2013. Paradoxical role of the proto-oncogene Axl and Mer receptor tyrosine kinases in colon cancer. *Proc Natl Acad Sci U S A*. 110:13091–13096.

Brázda V, Laister RC, Jagelská EB, Arrowsmith C. 2011. Cruciform structures are a common DNA feature important for regulating biological processes. *BMC Mol Biol*. 12:33.

Brea-Fernández AJ, Pomares E, Brión MJ, Marfany G, Blanco MJ, Sánchez-Salorio M, González-Duarte R, Carracedo A. 2008. Novel splice donor site mutation in MERTK gene associated with retinitis pigmentosa. *Br J Ophthalmol*. 92:1419–1423.

Brunet FG, Volff J-N, Schartl M. 2016. Whole genome duplications shaped the receptor tyrosine kinase repertoire of jawed vertebrates. *Genome Biol Evol*. 8:1600–1613.

Buckling A, Wei Y, Massey RC, Brockhurst MA, Hochberg ME. 2006. Antagonistic coevolution with parasites increases the cost of host deleterious mutations. *Proc Biol Sci*. 273:45–49.

Caetano FA, Dirk BS, Tam JHK, Cavanagh PC, Goiko M, Ferguson SSG, Pasternak SH, Dikeakos JD, de Bruyn JR, Heit B. 2015. MIiSR: molecular interactions in super-resolution imaging enables the analysis of protein interactions, dynamics and formation of multi-protein structures. *PLoS Comput Biol*. 11:e1004634.

Cavalli M, Pan G, Nord H, Wallén Arzt E, Wallerman O, Wadelius C. 2016. Genetic prevention of hepatitis C virus-induced liver fibrosis by allele-specific downregulation of MERTK. *Hepatol Res*. 1–5.

Chen Y, Wang H, Qi N, Wu H, Xiong W, Ma J, Lu Q, Han D. 2009. Functions of TAM RTKs in regulating spermatogenesis and male fertility in mice. *Reproduction* 138:655–666.

Clark K, Karsch-Mizrachi I, Lipman DJ, Ostell J, Sayers EW. 2016. GenBank. *Nucleic Acids Res*. 44:D67–D72.

Dahlmann F, Biedenkopf N, Babler A, Jahnen-Dechent W, Karsten CB, Gnirß K, Schneider H, Wrensch F, O'Callaghan CA, Bertram S, et al. 2015. Analysis of Ebola virus entry into macrophages. *J Infect Dis*. 212:S247–S257.

Dawkins R, Leelayuwat C, Gaudieri S, Tay G, Hui J, Cattley S, Martinez P, Kulski J. 1999. Genomics of the major histocompatibility complex: haplotypes, duplication, retroviruses and disease. *Immunol Rev*. 167:275–304.

Dean AM, Neuhauser C, Grenier E, Golding GB. 2002. The pattern of amino acid replacements in alpha/beta-barrels. *Mol Biol Evol*. 19:1846–1864.

Doron-Faigenboim A, Stern A, Mayrose I, Bacharach E, Pupko T. 2005. Selection: A server for detecting evolutionary forces at a single amino-acid site. *Bioinformatics* 21:2101–2103.

Doxiadis GGM, de Groot N, Bontrop RE. 2008. Impact of endogenous intronic retroviruses on major histocompatibility complex class II diversity and stability. *J Virol*. 82:6667–6677.

Duncan JL, LaVail MM, Yasumura D, Matthes MT, Yang H, Trautmann N, Chappelow AV, Feng W, Earp HS, Matsushima GK, et al. 2003. An RCS-like retinal dystrophy phenotype in Mer knockout mice. *Investig Ophthalmol Vis Sci*. 44:826–838.

Emes RD, Yang Z. 2008. Duplicated paralogous genes subject to positive selection in the genome of *Trypanosoma brucei*. *PLoS One* 3:e2295.

Evans AL, Blackburn JWD, Yin C, Heit B. 2017. Quantitative efferocytosis assays. *Methods Mol Biol*. 1519:25–41.

Gaboriaud C, Bissery V, Benchetrit T, Mornon JP. 1987. Hydrophobic cluster analysis: an efficient new way to compare and analyse amino acid sequences. *FEBS Lett*. 224:149–155.

Gibson DG, Young L, Chuang R-Y, Venter JC, Hutchison CA, Smith HO. 2009. Enzymatic assembly of DNA molecules up to several hundred kilobases. *Nat Methods* 6:343–345.

Goiko M, de Bruyn JR, Heit B. 2016. Short-lived cages restrict protein diffusion in the plasma membrane. *Sci Rep*. 6:34987.

Grabiec AM, Hussell T. 2016. The role of airway macrophages in apoptotic cell clearance following acute and chronic lung inflammation. *Semin Immunopathol*. 38(4):409–423.

Graham DK, Dawson TL, Mullaney DL, Snodgrass HR, Earp HS. 1994. Cloning and mRNA expression analysis of a novel human protooncogene, c-mer. *Cell Growth Differ*. 5:647–657.

Graham DK, DeRyckere D, Davies KD, Earp HS. 2014. The TAM family: phosphatidylserine-sensing receptor tyrosine kinases gone awry in cancer. *Nat Rev Cancer* 14:769–785.

Gralle M, Pääbo S. 2011. A comprehensive functional analysis of ancestral human signal peptides. *Mol Biol Evol*. 28:25–28.

Grommes C, Lee CYD, Wilkinson BL, Jiang Q, Koenigsknecht-Talboo JL, Varnum B, Landreth GE. 2008. Regulation of microglial phagocytosis and inflammatory gene expression by Gas6 acting on the Axl/Mer family of tyrosine kinases. *J Neuroimmune Pharmacol*. 3:130–140.

Healy LM, Perron G, Won S-Y, Michell-Robinson MA, Rezk A, Ludwin SK, Moore CS, Hall JA, Bar-Or A, Antel JP. 2016. MerTK is a functional regulator of myelin phagocytosis by human myeloid cells. *J Immunol*. 196(8):3375–3384.

Heit B, Kim H, Cosío G, Castaño D, Collins R, Lowell CA, Kain KC, Trimble WS, Grinstein S. 2013. Multimolecular signaling complexes enable Syk-mediated signaling of CD36 internalization. *Dev Cell* 24:372–383.

Hellberg ME, Moy GW, Vacquier VD. 2000. Positive selection and propeptide repeats promote rapid interspecific divergence of a gastropod sperm protein. *Mol Biol Evol*. 17:458–466.

Heredia A, Gilliam B, DeVico A, Le N, Bamba D, Flinko R, Lewis G, Gallo RC, Redfield RR. 2007. CCR5 density levels on primary CD4 T cells impact the replication and Enfuvirtide susceptibility of R5 HIV-1. *AIDS* 21:1317–1322.

Hughes JF, Coffin JM. 2001. Evidence for genomic rearrangements mediated by human endogenous retroviruses during primate evolution. *Nat Genet*. 29:487–489.

Hurtado BB, Abasolo N, Muñoz X, García N, Benavente Y, Rubio F, De Frutos PG, Krupinski J, Sala NN, Muñoz X, et al. 2010. Association study between polymorphims in GAS6-TAM genes and carotid atherosclerosis. *Thromb Haemost*. 104:592–598.

Ishimoto Y, Ohashi K, Mizuno K, Nakano T. 2000. Promotion of the uptake of PS liposomes and apoptotic cells by a product of growth arrest-specific gene, gas6. *J Biochem*. 127:411–417.

Kelley LA, Mezulis S, Yates CM, Wass MN, Sternberg MJE. 2015. The Phyre2 web portal for protein modeling, prediction and analysis. *Nat Protoc*. 10:845–858.

Kim EL, Peng H, Esparza FM, Maltchenko SZ, Stachowiak MK. 1998. Cruciform-extruding regulatory element controls cell-specific activity of the tyrosine hydroxylase gene promoter. *Nucleic Acids Res*. 26:1793–1800.

Kimani SG, Kumar S, Davra V, Chang Y-J, Kasikara C, Geng K, Tsou W-I, Wang S, Hoque M, Boháč A, et al. 2016. Normalization of TAM post-receptor signaling reveals a cell invasive signature for Axl tyrosine kinase. *Cell Commun Signal*. 14:19.

van Kooyk Y, van Vliet SJ, Figdor CG. 1999. The actin cytoskeleton regulates LFA-1 ligand binding through avidity rather than affinity changes. *J Biol Chem*. 274:26869–26877.

Kyte J, Doolittle RF. 1982. A simple method for displaying the hydropathic character of a protein. *J Mol Biol*. 157:105–132.

Leabman MK, Huang CC, DeYoung J, Carlson EJ, Taylor TR, de la Cruz M, Johns SJ, Stryke D, Kawamoto M, Urban TJ, et al. 2003. Natural variation in human membrane transporter genes reveals evolutionary and functional constraints. *Proc Natl Acad Sci U S A*. 100:5896–5901.

Lee Y-J, Han J-Y, Byun J, Park H-JH-JH-J, Park E-ME-ME-M, Chong YH, Cho M-SM-S, Kang JL. 2012. Inhibiting Mer receptor tyrosine kinase suppresses STAT1, SOCS1/3, and NF-κB activation and enhances inflammatory responses in lipopolysaccharide-induced acute lung injury. *J Leukoc Biol*. 91:921–932.

Lee YH, Ota T, Vacquier VD. 1995. Positive selection is a general phenomenon in the evolution of abalone sperm lysin. *Mol Biol Evol*. 12:231–238.

Lemke G, Rothlin CV. 2008. Immunobiology of the TAM receptors. *Nat Rev Immunol*. 8:327–336.

Li E, Wimley WC, Hristova K. 2012. Transmembrane helix dimerization: beyond the search for sequence motifs. *Biochim Biophys Acta* 1818:183–193.

Li Q, Lu QQ, Lu H, Tian S, Lu QQ. 2013. Systemic autoimmunity in TAM triple knockout mice causes inflammatory brain damage and cell death. *PLoS One* 8:e64812.

Li Y-D, Xie Z-Y, Du Y-L, Zhou Z, Mao X-M, Lv L-X, Li Y-Q. 2009. The rapid evolution of signal peptides is mainly caused by relaxed selection on non-synonymous and synonymous sites. *Gene* 436:8–11.

Linger RMA, Keating AK, Earp HS, Graham DK. 2008. TAM receptor tyrosine kinases: biologic functions, signaling, and potential therapeutic targeting in human cancer. *Adv Cancer Res*. 100:35–83.

Lu Q, Gore M, Zhang Q, Camenisch T, Boast S, Casagranda F, Lai C, Skinner MK, Klein R, Matsushima GK, et al. 1999. Tyro-3 family receptors are essential regulators of mammalian spermatogenesis. *Nature* 398:723–728.

Ma GZM, Stankovich J, Kilpatrick TJ, Binder MD, Field J. 2011. Polymorphisms in the receptor tyrosine kinase MERTK gene are associated with multiple sclerosis susceptibility. *PLoS One* 6:e16964.

McNatt MW, Zang T, Hatziioannou T, Bartlett M, Fofana IB, Johnson WE, Neil SJD, Bieniasz PD. 2009. Species-specific activity of HIV-1 Vpu and positive selection of tetherin transmembrane domain variants. *PLoS Pathog*. 5:e1000300.

Mokrab Y, Stevens TJ, Mizuguchi K. 2010. A structural dissection of amino acid substitutions in helical transmembrane proteins. *Proteins Struct Funct Bioinformatics* 78:2895–2907.

Morizono K, Xie Y, Olafsen T, Lee B, Dasgupta A, Wu AM, Chen ISY. 2011. The soluble serum protein Gas6 bridges virion envelope phosphatidylserine to the TAM receptor tyrosine kinase Axl to mediate viral entry. *Cell Host Microbe* 9:286–298.

Nguyen K-QN, Tsou W-I, Calarese D. a, Kimani SG, Singh S, Hsieh S, Liu Y, Lu B, Wu Y, Garforth SJ, et al. 2014. Overexpression of MERTK receptor tyrosine kinase in epithelial cancer cells drives efferocytosis in a gain-of-function capacity. *J Biol Chem*. 289:25737–25749.

Noda T, Sagara H, Suzuki E, Takada A, Kida H, Kawaoka Y. 2002. Ebola virus VP40 drives the formation of virus-like filamentous particles along with GP. *J Virol*. 76:4855–4865.

Nordbotten JM, Stenseth NC. 2016. Asymmetric ecological conditions favor Red-Queen type of continued evolution over stasis. *Proc Natl Acad Sci U S A*. 113:1847–1852.

O'Leary NA, Wright MW, Brister JR, Ciufo S, Haddad D, McVeigh R, Rajput B, Robbertse B, Smith-White B, Ako-Adjei D, et al. 2016. Reference sequence (RefSeq) database at NCBI: current status, taxonomic expansion, and functional annotation. *Nucleic Acids Res*. 44:D733–D745.

Ortiz M, Guex N, Patin E, Martin O, Xenarios I, Ciuffi A, Quintana-Murci L, Telenti A. 2009. Evolutionary trajectories of primate genes involved in HIV pathogenesis. *Mol Biol Evol*. 26:2865–2875.

Paterson S, Vogwill T, Buckling A, Benmayor R, Spiers AJ, Thomson NR, Quail M, Smith F, Walker D, Libberton B, et al. 2010. Antagonistic coevolution accelerates molecular evolution. *Nature* 464:275–278.

Perros M, Spegelaere P, Dupont F, Vanacker JM, Rommelaere J. 1994. Cruciform structure of a DNA motif of parvovirus minute virus of mice (prototype strain) involved in the attenuation of gene expression. *J Gen Virol*. 75 (Pt 10): 2645–2653.

Read SA, Tay ES, Shahidi M, O'Connor KS, Booth DR, George J, Douglas MW. 2015. Hepatitis C virus driven AXL expression suppresses the hepatic type i interferon response. *PLoS One* 10:e0136227.

Rothlin CV, Ghosh S, Zuniga EI, Oldstone MBA, Lemke G. 2007. TAM receptors are pleiotropic inhibitors of the innate immune response. *Cell* 131:1124–1136.

Sabeti PC, Varilly P, Fry B, Lohmueller J, Hostetter E, Cotsapas C, Xie X, Byrne EH, McCarroll SA, Gaudet R, et al. 2007. Genome-wide detection and characterization of positive selection in human populations. *Nature* 449:913–918.

Sasaki T, Knyazev PG, Clout NJ, Cheburkin Y, Göhring W, Ullrich A, Timpl R, Hohenester E. 2006. Structural basis for Gas6-Axl signalling. *EMBO J* 25:80–87.

Sawyer SL, Wu LI, Emerman M, Malik HS. 2005. Positive selection of primate TRIM5alpha identifies a critical species-specific retroviral restriction domain. *Proc Natl Acad Sci U S A*. 102:2832–2837.

Shelby SJ, Colwill K, Dhe-Paganon S, Pawson T, Thompson D. a. 2013. MERTK Interactions with SH2-domain proteins in the retinal pigment epithelium. *PLoS One* 8:e53964.

Shibata T, Habiel DM, Coelho AL, Kunkel SL, Lukacs NW, Hogaboam CM. 2014. Axl receptor blockade ameliorates pulmonary pathology resulting from primary viral infection and viral exacerbation of asthma. *J Immunol*. 192:3569–3581.

Shimojima M, Takada A, Ebihara H, Neumann G, Fujioka K, Irimura T, Jones S, Feldmann H, Kawaoka Y. 2006. Tyro3 family-mediated cell entry of Ebola and Marburg viruses. *J Virol*. 80:10109–10116.

Singer MS, Weisinger-Lewin Y, Lancet D, Shepherd GM. 1996. Positive selection moments identify potential functional residues in human olfactory receptors. *Receptors Channels* 4:141–147.

Stanford JC, Young C, Hicks D, Owens P, Williams A, Vaught DB, Morrison MM, Lim J, Williams M, Brantley-sieders DM, et al. 2014. Efferocytosis produces a prometastatic landscape during postpartum mammary gland involution. *J Clin Invest*.124:4737–4752.

Steiger SS, Fidler AE, Mueller JC, Kempenaers B. 2010. Evidence for adaptive evolution of olfactory receptor genes in 9 bird species. *J Hered*. 101:325–333.

Stevens TJ, Arkin IT. 2001. Substitution rates in alpha-helical transmembrane proteins. *Protein Sci*. 10:2507–2517.

Subramanian M, Proto JD, Matsushima GK, Tabas I. 2016. Deficiency of AXL in bone marrow-derived cells does not affect advanced atherosclerotic lesion progression. *Sci Rep*. 6:39111.

Tamura K, Stecher G, Peterson D, Filipski A, Kumar S. 2013. MEGA6: Molecular Evolutionary Genetics Analysis Version 6.0. *Mol Biol Evol*. 30:2725–2729.

Thorp E, Cui D, Schrijvers DM, Kuriakose G, Tabas I. 2008. Mertk receptor mutation reduces efferocytosis efficiency and promotes apoptotic cell accumulation and plaque necrosis in atherosclerotic lesions of apoe−/− mice. *Arterioscler Thromb Vasc Biol*. 28:1421–1428.

Tibrewal N, Wu Y, D'mello V, Akakura R, George TC, Varnum B, Birge RB. 2008. Autophosphorylation docking site Tyr-867 in Mer receptor tyrosine kinase allows for dissociation of multiple signaling pathways for phagocytosis of apoptotic cells and down-modulation of lipopolysaccharide-inducible NF-kappaB transcriptional activation. *J Biol Chem*. 283:3618–3627.

Tsou W-I, Nguyen K-QN, Calarese D. a, Garforth SJ, Antes AL, Smirnov SV, Almo SC, Birge RB, Kotenko SV. 2014. Receptor tyrosine kinases, TYRO3, AXL, and MER, demonstrate distinct patterns and complex regulation of ligand-induced activation. *J Biol Chem*. 289:25750–25763.

Van Valen L. 1973. A new evolutionary law. *Evol Theory* 1:1–30.

Vallender EJ, Lahn BT. 2004. Positive selection on the human genome. *Hum Mol Genet*. 13:245–254.

Wallet M. A, Sen P, Flores RR, Wang Y, Yi Z, Huang Y, Mathews CE, Earp HS, Matsushima G, Wang B, et al. 2008. MerTK is required for apoptotic cell-induced T cell tolerance. *J Exp Med*. 205:219–232.

Wan E, Yeap X-YY, Dehn S, Terry R, Novak M, Zhang S, Iwata S, Han X, Homma S, Drosatos K, et al. 2013. Enhanced efferocytosis of apoptotic cardiomyocytes through myeloid-epithelial-reproductive tyrosine kinase links acute inflammation resolution to cardiac repair after infarction. *Circ Res*. 113:1004–1012.

Wang Z, Zhong M, Fu M, Dou T, Bian Z. 2014. Evidence of positive selection at signal peptide region of interferon gamma. *Biosc. Biotechnol Biochem*. 78:588–592.

Watanabe S, Watanabe T, Noda T, Takada A, Feldmann H, Jasenosky LD, Kawaoka Y. 2004. Production of novel ebola virus-like particles from cDNAs: an alternative to ebola virus generation by reverse genetics. *J Virol*. 78:999–1005.

Weinger JG, Gohari P, Yan Y, Backer JM, Varnum B, Shafit-Zagardo B. 2008. In brain, Axl recruits Grb2 and the p85 regulatory subunit of PI3 kinase; in vitro mutagenesis defines the requisite binding sites for downstream Akt activation. *J Neurochem*. 106:134–146.

Williams EJB, Pal C, Hurst LD. 2000. The molecular evolution of signal peptides. *Gene* 253:313–322.

Williamson SH, Hubisz MJ, Clark AG, Payseur BA, Bustamante CD, Nielsen R. 2007. Localizing recent adaptive evolution in the human genome. *PLoS Genet*. 3:901–915.

Yohn CT, Jiang Z, McGrath SD, Hayden KE, Khaitovich P, Johnson ME, Eichler MY, McPherson JD, Zhao S, Pääbo S, et al. 2005. Lineage-specific expansions of retroviral insertions within the genomes of African great apes but not humans and orangutans. *PLoS Biol*. 3:e110.

Zagórska A, Través PG, Lew ED, Dransfield I, Lemke G. 2014. Diversification of TAM receptor tyrosine kinase function. *Nat Immunol*. 15:920–928.

Zhang B, Fang L, Wu H-M, Ding P-S, Xu K, Liu R-Y. 2016. Mer receptor tyrosine kinase negatively regulates lipoteichoic acid-induced inflammatory response via PI3K/Akt and SOCS3. *Mol Immunol*. 76:98–107.

Zizzo G, Hilliard BA, Monestier M, Cohen PL. 2012. Efficient clearance of early apoptotic cells by human macrophages requires M2c polarization and MerTK induction. *J Immunol*. 189:3508–3520.